Journal of Fluorescence, Vol. 2, No. 1, 1992

Calcium Imaging Using Fluorescence Lifetimes and Long-Wavelength Probes

Joseph R. Lakowicz,[1,3] Henryk Szmacinski,[1] and Michael L. Johnson[2]

Received February 6, 1992; revised May 12, 1992; accepted June 8, 1992

We describe imaging of calcium concentrations using the long-wavelength Ca^{2+} indicators, Calcium Green, Orange, and Crimson. The lifetimes of these probes were measured using the frequency-domain method and were found to increase from 50% to severalfold in response to calcium. The two-dimensional images of the calcium concentration were obtained using a new apparatus for fluorescence lifetime imaging (FLIM). We also describe procedures to correct for the position-dependent frequency response of the gain-modulated image intensifier used in the FLIM apparatus. Importantly, the FLIM method does not require the probe to display shifts in the excitation or emission spectra. Using the FLIM method, calcium imaging is possible using probes which display changes in lifetime in response to calcium. Consequently, calcium imaging is possible with excitation wavelengths ranging from 488 to as long as 620 nm, where autofluorescence and/or photochemical damage is minimal. These probes are also suitable for calcium measurements of single cells using lifetime-based flow cytometry.

KEY WORDS: Calcium; fluorescence lifetime imaging; calcium imaging; fluorescence microscopy; ratiometric imaging; long-wavelength probes.

INTRODUCTION

Measurements of the intracellular concentrations of Ca^{2+} are of considerable interest in biochemistry and cell physiology. The intracellular concentration of free Ca^{2+} is tightly regulated and cannot be determined by disruptive methods. Consequently, most measurements of intracellular calcium or Ca^{2+} imaging are performed using fluorescence indicators (1–3), such as Quin-2 and Fura-2, which change intensity in response to Ca^{2+}. The second-generation dye Fura-2 is currently preferred for a variety of chemical and biochemical reasons (3,4). The primary advantage of Fura-2 over Quin-2 appears to be the shift in its excitation wavelength in response to Ca^{2+} (5–7), which allows calculation of the calcium concentration from the ratio of the fluorescence intensities at two excitation wavelengths, thus providing a measure of the $[Ca^{2+}]$ which is independent of the probe concentration.

A disadvantage of both Fura-2 and Quin-2 is the need for UV excitation in the range 330–360 nm. These wavelengths are undesirable due to the simultaneous excitation of autofluorescence from unknown cellular fluorophores and known species such as NADH, the poor transmission of these wavelengths through microscope optics, and the expense of UV laser sources. In addition, the need for UV excitation precludes the use of Fura-2 and Quin-2 with caged Ca^{2+} complexes which release Ca^{2+} in response to UV illumination (8–10). In order to circumvent these difficulties, a new series of calcium

[1] Center for Fluorescence Spectroscopy, Department of Biological Chemistry, University of Maryland at Baltimore, 660 West Redwood Street, Baltimore, Maryland 21201.
[2] University of Virginia, Department of Pharmacology, Charlottesville, Virginia 22908.
[3] To whom correspondence should be addressed.

1053-0509/92/0300-0047$06.50/0

probes has been developed by Molecular Probes (11). These probes, called Calcium Green (CaG),[4] Calcium Orange (CaO), and Calcium Crimson (CaC), have absorption maximum at 508, 552, and 590 nm, respectively, and still longer excitation wavelengths could be used on the long-wavelength sides of the absorption. The chemical structures of these probes have only recently become available (12) and are shown in Scheme I. These probes are conjugates of 2′,7′-dichloro-5-carboxyfluorescein, tetramethylrhodamine-6-isothiocyanate (TRITC), and Texas red sulfonyl chloride, with the calcium chelator, 5′-amino-1,2-bis(2-aminophenoxy)ethane-*N,N,N′,N′*-tetraacetic acid (5′-amino BAPTA). However, using the presently available methods of fluorescence microscopy, these probes cannot be considered to be substitutes for Fura-2 because there are no shifts in their excitation or emission wavelengths in response to Ca^{2+}.

In the present report we describe the use of Calcium Green, Orange, and Crimson for imaging of calcium concentrations without the need for wavelength-ratiometric methods. We found that the fluorescence lifetimes of these probes increase upon Ca^{2+} binding. We used a new imaging methodology, fluorescence lifetime imaging (FLIM), in which the fluorescence lifetime at each pixel is used to create the image contrast. The FLIM apparatus is a frequency-domain device (13,14) which uses a gain-modulated image intensifier (15,16), allowing simultaneous acquisition of the lifetime information at all pixels in the image. Importantly, lifetimes are absolute rather than relative quantities, so that these FLIM measurements do not require additional calibration.

PRINCIPLE OF FLUORESCENCE LIFETIME IMAGING

The concept of fluorescence lifetime imaging is shown schematically in Fig. 1. At present the FLIM apparatus has not yet been adapted in a microscope, so that the "object" consists of a row of four to six cuvettes, each containing the calcium indicator and different concentrations of free Ca^{2+}. Observation of the intensity image will not reveal calcium concentrations unless the indicator concentration is known, which is generally not possible in a microscopic sample. However, fluorescence lifetimes are independent of the local probe concentration, providing that the measurements are within the dynamic range of the apparatus and the fluorophores are not so concentrated as to display self-quenching effects. Hence, for a suitable probe, the lifetime provides a measure of the calcium concentration in each cuvette and/or region of the image.

To create the FLIM images we use the image intensifier as a two-dimensional (2D) phase-sensitive detector, in which the signal intensity at each position (r) depends on the phase angle difference between the emission and the gain modulation of the detector. This results in a constant intensity which is proportional both to the concentration of the fluorophore (C) at location r [$C(r)$] and to the cosine of the phase angle difference,

$$I(\theta_D, r) = kC(r) \left[1 + \frac{1}{2} m_D(r) m(r) \cos[\theta_{obs}(r) - \theta_D(r)]\right] \quad (1)$$

In this expression $\theta_D(r)$ is the phase of the gain modulation and $\theta_{obs}(r)$ is the phase angle of the fluorescence, $m(r)$ is the modulation of the fluorescence, and $m_D(r)$ is the gain modulation of the detector. This term $m_D(r)$ also contains a factor proportional to the extent of modulation of the incident light. In this expression $\theta_D(r) = 0$ corresponds to the detector being in phase with scattered light, that is, a lifetime of zero.

The lifetime image cannot be calculated from a single phase-sensitive image. However, the phase of the emission can be determined by examining its dependency on the detector phase angle dependence of the emission [Eq. (1)], which can be accomplished by a series of electronic delays. We collect a series of phase-sensitive images (Fig. 1), in which $\theta_D(r)$ is varied over 360° or more. The phase-sensitive intensities at each pixel are used to determine the phase at each pixel.

We also use the spatially dependent modulation to create modulation or modulation-lifetime images. The modulation [$m_{em}(r)$] of the emission, relative to the observed modulation of a reference (R) solution [$m_R(r)$], is given by

$$m_{obs}(r) = \frac{m_{em}(r)}{m_R(r)} \quad (2)$$

In the present measurements we used the phase (θ_R) and modulation (m_R) of the Ca^{2+}-saturated sample as the reference, as shown previously for lifetime standards (17).

[4] Abbreviations used: CaG, CaO, and CaC, Calcium Green, Orange, and Crimson, trademarks of Molecular Probes, Eugene, OR 97402; CCD, charged-coupled device; FD, frequency domain; FLIM, fluorescence lifetime imaging; Fura-2, 2-(6-bis(carboxymethyl)amino)-5-(2-(2-(bis(carboxymethyl)amino)-5-methylphenoxy)ethoxy-2-benzofuranyl-5-oxazolecarboxylic acid; MCP, microchannel plate; Quin-2, 2-{[2-bis-(carboxymethyl)-amino-5-methylphenoxyl]-methyl}-6-methoxy-8-bis-(carboxymethyl)-aminoquinoline

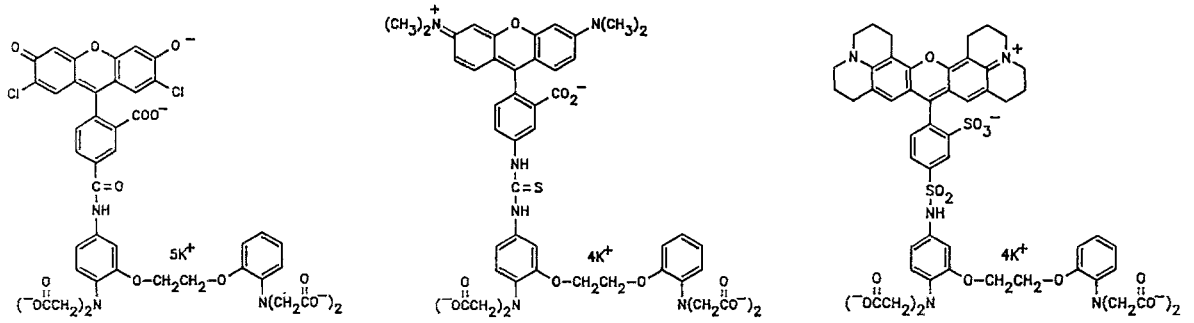

Calcium Green Calcium Orange Calcium Crimson

Scheme I. Chemical structures of Calcium Green (CaG), Orange (CaO), and Crimson (CaC).

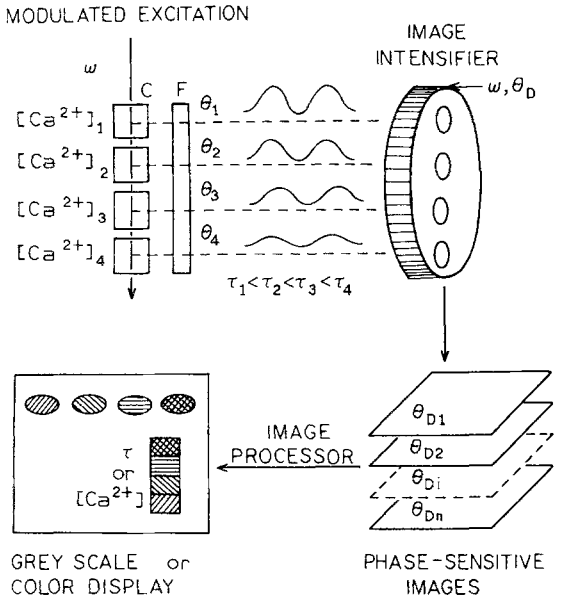

Fig. 1. Intuitive schematic of fluorescence lifetime imaging of calcium.

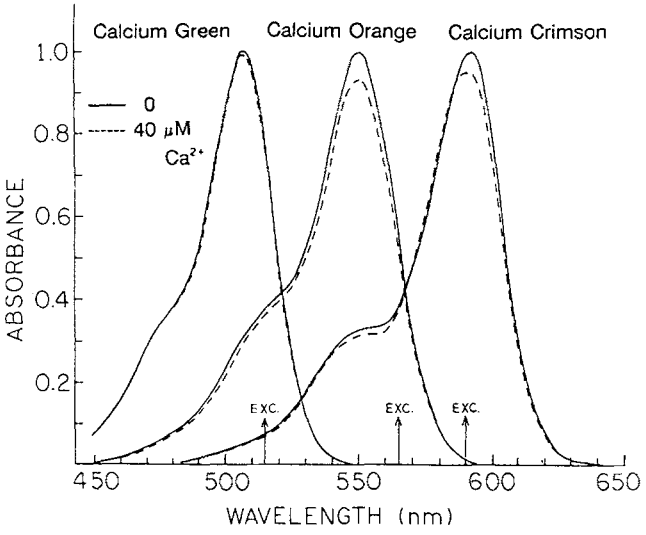

Fig. 2. Absorption spectra of Calcium Orange, Green, and Crimson.

These phase and modulation values were determined using standard frequency-domain measurements (13,14, 18,19) of the same samples. The true value of the modulation at each point in the image, corrected for the nonzero lifetime of the reference (τ_R), is given by

$$m(r) = \frac{m_{obs}(r)}{\sqrt{1 + \omega^2\tau_R^2}} \tag{3}$$

where $m_{obs}(r)$ is the observed modulation relative to the reference sample or region of the image (17). Similarly the phase angle of the sample, corrected for the phase angle of the reference, is given by

$$\theta(r) = \theta_{obs}(r) + \theta_R \tag{4}$$

where $\theta_{obs}(r)$ is the phase angle observed relative to the reference, and θ_R = atan ($\omega\tau_R$) is the phase angle of the reference relative to the excitation. These phase and modulation images can be transformed to lifetime images. The phase angle of the fluorescence is related to the apparent phase lifetime τ_θ and the light modulation frequency (ω, in radians/s) by

$$\tau_\theta(r) = \frac{1}{\omega} \tan \theta(r) \tag{5}$$

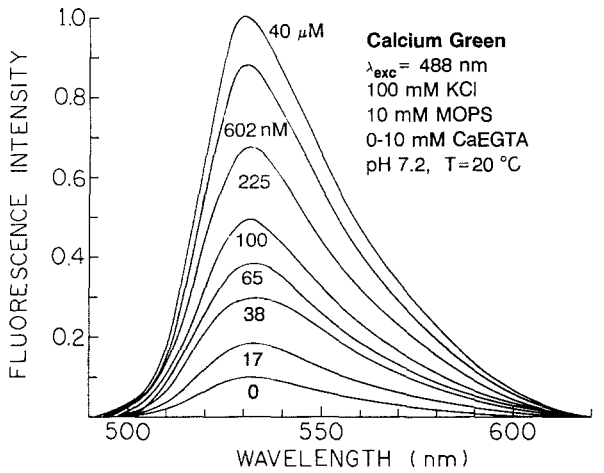

Fig. 3. Calcium-dependent emission spectra of Calcium Green.

The apparent modulation lifetime image is given by

$$\tau_m(r) = \frac{1}{\omega}\sqrt{\frac{1}{m^2(r)} - 1} \qquad (6)$$

EXPERIMENTAL

FLIM Instrumentation

A detailed description of the FLIM apparatus is given elsewhere (15,16). The light source is a ps dye laser system, consisting of a mode-locked argon ion or Antares Nd:YAG laser, which synchronously pumps a cavity-dumped dye laser containing rhodamine 6G. CaC and CaO were excited with the dye laser output at 565 or 590 nm, respectively, with a repetition rate of 3.81 MHz. Phase and modulation measurements can be performed at any integer multiple of the cavity-dumped repetition rate of 3.81 MHz (20). CaG was excited with the 514.5 nm output of the argon ion or the 532-nm output of the Nd:YAG with mode-locked repetition rates of 75.9 and 76.2 MHz, respectively.

The gated image intensifier was positioned between the target and a CCD camera. The intensifier gain was modulated by a RF signal applied between the photocathode and the microchannel plate (MCP) input surface. The detector was a CCD camera from Photometrics (Series 200) with a thermoelectrically cooled PM-512 CCD. In the early measurements, phase delays were introduced into this gating signal using calibrated coaxial cables. We subsequently installed a PTS 300 frequency synthesizer which allows the output phase to be changed electronically under control of an IBM/PC and an IEEE interface. Identical results were obtained for the cable and electronic phase shifts, except that the latter allowed for more rapid data acquisition.

The phase-sensitive images are rather large (512 × 512 pixels and 520-kbyte storage for each image). To allow rapid calculation of images we developed a noninteractive algorithm which uses each image or region of an image only one time (16). This algorithm (CCDFT) calculates the phase and modulation at each pixel, using the phase-sensitive images obtained with various detec-

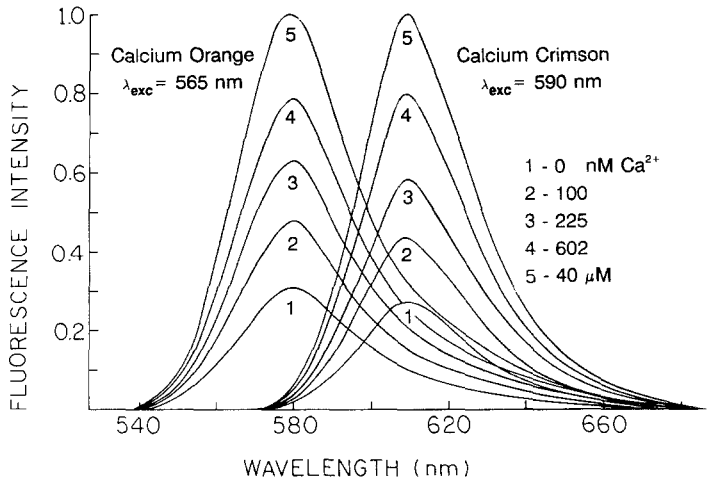

Fig. 4. Calcium-dependent emission spectra of Calcium Orange and Crimson.

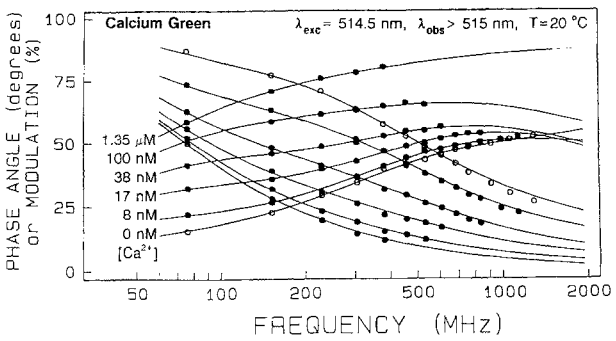

Fig. 5. Frequency-response of Calcium Green with increasing concentrations of calcium.

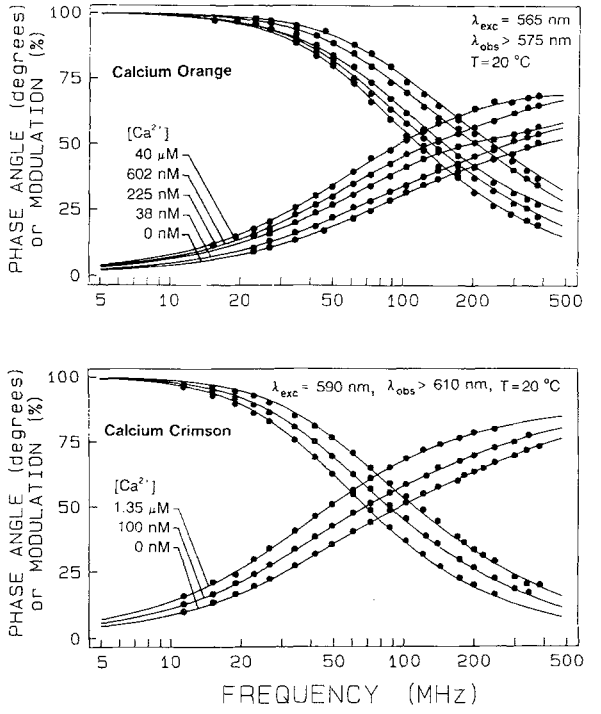

Fig. 6. Frequency-response of Calcium Orange (top) and Calcium Crimson (bottom) with increasing amounts of calcium.

Table I. Multiexponential Analysis of the Intensity Decay of Calcium Green[a]

$[Ca^{2+}]$	$\bar{\tau}$ (ns)[b]	τ_i (ns)	α_i	f_i	χ^2_R
0		0.11	0.751	0.30	
	—	0.79	0.249	0.70	46.8[c] (988)[d]
		0.05	0.663	0.157	
		0.45	0.319	0.621	
	0.92	2.88	0.018	0.322	4.2
8 n*M*		0.16	0.820	0.327	
	—	1.51	0.180	0.673	106.3 (1706)
		0.03	0.742	0.100	
		0.43	0.236	0.501	
	1.68	3.65	0.022	0.399	2.7
17 n*M*		0.23	0.826	0.283	
	—	2.75	0.173	0.717	48.2 (2323)
		0.01	0.895	0.059	
		0.44	0.085	0.327	
	2.35	3.58	0.020	0.615	1.3
38 n*M*		0.27	0.748	0.183	
	—	3.34	0.252	0.807	18.4 (2361)
		0.02	0.829	0.044	
		0.48	0.115	0.200	
	2.90	3.72	0.056	0.756	2.4
65 n*M*		0.27	0.660	0.131	
	—	3.45	0.340	0.869	4.9 (1902)
		0.02	0.692	0.023	
		0.38	0.177	0.124	
	3.08	3.55	0.131	0.853	1.6
100 n*M*		0.30	0.543	0.091	
	—	3.57	0.457	0.909	7.7 (1140)
		0.02	0.729	0.023	
		0.55	0.114	0.094	
	3.35	3.74	0.157	0.883	2.8
225 n*M*		0.40	0.378	0.062	
	3.51	3.71	0.621	0.938	2.1 (426)
602 n*M*		0.57	0.199	0.036	
	3.64	3.76	0.801	0.964	1.8 (88)
1.35 μ*M*		0.68	0.143	0.030	
	3.65	3.74	0.857	0.970	0.8 (37)
40 μ*M*		0.70	0.142	0.030	
	3.68	3.77	0.857	0.970	2.4 (34)

[a] Excitation, 514.5 nm, argon ion laser; emission filter, Corning 3-69; buffer, 100 m*M* KCl, 10 m*M* MOPS, 0–10 m*M* CaEGTA, pH 7.2, 20°C.

[b] $\bar{\tau} = \Sigma f_i \tau_i$.

[c] $\delta\phi = 0.3°$ and $\delta m = 0.005$.

[d] The values in parentheses are the χ^2_R values from the single-decay time fits.

tor phase angles [Eq. (1)]. The FLIM algorithm (16) has been modified because of an intensity-dependent bias in the calculated lifetimes. The phase of the detector is generally shifted relative to that of the modulated excitation (θ_I) due to time delays throughout the apparatus. In the present report, the detector phase angles are given as $\theta' = \theta_D + \theta_I$, where θ_I is the phase shift intrinsic to the apparatus. Calculation of the phase angle or lifetime of the emission requires correction of the apparent phase angles for this instrumental shift.

And, finally, we note that the experiments were performed with six cuvettes which were imaged over the entire diameter of the image intensifier. Hence, in contrast to our earlier measurements (16,21), it was necessary to correct the present data for the time- and position-

Table II. Global Multiexponential Analysis of the Intensity Decay of Calcium Green[a]

Double-exponential fit: $\chi^2_R = 86.2$, $\tau_2 = 0.24$ ns, $\tau_2 = 3.28$ ns

Triple-exponential fit: $\chi^2_R = 2.8$, $\tau_1 = 0.05$ ns, $\tau_2 = 0.45$ ns, $\tau_3 = 3.66$ ns

$[Ca^{2+}]$	α_1	α_2	α_3	f_1	f_2	f_3	$\bar{\tau}$ (ns)
0	0.958	0.042	—	0.625	0.375	—	1.38
	0.681	0.307	0.012	0.150	0.651	0.200	1.05
4 n*M*	0.941	0.059	—	0.536	0.464	—	1.64
	0.686	0.294	0.021	0.133	0.550	0.317	1.42
8 n*M*	0.924	0.076	—	0.471	0.529	—	1.85
	0.674	0.296	0.029	0.116	0.490	0.394	1.66
17 n*M*	0.849	0.151	—	0.291	0.709	—	2.39
	0.637	0.293	0.070	0.071	0.315	0.614	2.39
38 n*M*	0.745	0.255	—	0.176	0.824	—	2.74
	0.607	0.262	0.131	0.045	0.189	0.766	2.89
65 n*M*	0.653	0.347	—	0.121	0.879	—	2.91
	0.571	0.235	0.194	0.032	0.126	0.842	3.14
100 n*M*	0.534	0.466	—	0.077	0.923	—	3.04
	0.485	0.244	0.291	0.019	0.085	0.896	3.32
225 n*M*	0.355	0.645	—	0.039	0.961	—	3.16
	0.196	0.271	0.533	0.004	0.059	0.937	3.45
602 n*M*	0.166	0.834	—	0.014	0.986	—	3.24
	0.002	0.198	0.800	0.000	0.030	0.970	3.56
1.35 μ*M*	0.092	0.908	—	0.007	0.993	—	3.26
	0.011	0.118	0.871	0.000	0.016	0.984	3.61
40 μ*M*	0.087	0.913	—	0.007	0.993	—	3.26
	0.000	0.143	0.857	0.000	0.020	0.980	3.59

[a] See Table I footnotes for additional details.

Table III. Multiexponential Analysis of the Intensity Decay of Calcium Orange[a]

$[Ca^{2+}]$	$\bar{\tau}$ (ns)[b]	τ_i (ns)	α_i	f_i	χ^2_R
0		0.28	0.711	0.307	
	1.18	1.58	0.298	0.693	3.6[c] (325)[d]
		0.23	0.663	0.245	
		1.12	0.235	0.423	
	1.20	2.03	0.102	0.333	3.5
38 n*M*		0.37	0.698	0.312	
	1.42	1.89	0.301	0.688	2.2 (328)
		0.09	0.407	0.076	
		0.60	0.322	0.318	
	1.43	2.04	0.181	0.606	1.1
225 n*M*		0.30	0.629	0.191	
	1.78	2.13	0.371	0.809	2.9 (434)
		0.24	0.605	0.159	
		1.71	0.317	0.582	
	1.83	3.10	0.078	0.259	2.0
602 n*M*		0.46	0.510	0.168	
	2.05	2.37	0.490	0.832	1.8 (234)
		0.06	0.388	0.023	
		0.63	0.280	0.174	
	2.06	2.43	0.332	0.082	1.4
1.35 μ*M*		0.39	0.415	0.104	
	2.21	2.41	0.585	0.896	2.3 (158)
40 μ*M*		0.31	0.372	0.070	
	2.31	2.46	0.628	0.930	4.3 (128)
		0.05	0.547	0.029	
		0.075	0.093	0.070	
	2.31	2.51	0.359	0.901	3.1

[a] Excitation, 565 nm, R6G dye laser; emission filter, Corning 2-73; buffer, 100 m*M* KCl, 10 m*M* MOPS, 0–10 m*M* CaEGTA, pH 7.2 20°C.

[b] $\bar{\tau} = \Sigma f_i \tau_i$.

[c] $\delta\phi = 0.3°$ and $\delta m = 0.005$.

[d] The values in parentheses are the χ^2_R values from the single-decay time fits.

dependent response of the image intensifier. More specifically, we noticed that the phase angle of the gain modulation was not uniform across the intensifier and that the central region of the intensifier was delayed in phase relative to the regions near the outer circumference. The position-dependent shift in the intensifier was measured using a cylindrical tube containing a dilute solution of rhodamine 6G (R6G). The tube was positioned so that the laser beam propagated along its central axis. The lifetime is expected to be constant with distance so that the observed differences reflect the position-dependent response of the image intensifier. These values were used to correct the phase and modulation of the calcium indicator solutions by taking differences or ratios, respectively.

Frequency-Domain Measurements

Frequency-domain data were fit to the multiexponential model,

$$I(t) = \sum_{i=1}^{3} \alpha_i e^{-t/\tau_i} \tag{7}$$

where α_i are the preexponential factors and τ_i are the lifetimes (18,19). The intensity decays were also fit to a global model in which the decay times were assumed to be independent of Ca^{2+} concentration (k), but the values of α_{ik} to reflect changes in the fractional amounts preparation of each species. In this case the intensity decay at each Ca^{2+} concentration is given by

$$I_k(t) = \sum_{i=1}^{3} \alpha_{ik} e^{-t/\tau_i} \tag{8}$$

where the subscript k indicates the Ca^{2+} concentration. For the FLIM and FD measurements polarizers were not used to eliminate the effects of Brownian rotations, which are most probably insignificant for these decay times and viscosities. The excitation wavelengths and emission fil-

Table IV. Global Multiexponential Analysis of the Intensity Decay of Calcium Orange[a]

Double-exponential fit: $\chi_R^2 = 18.3$, $\tau_1 = 0.45$ ns, $\tau_2 = 2.34$ ns

Triple-exponential fit: $\chi_R^2 = 2.8$, $\tau_1 = 0.22$ ns, $\tau_2 = 1.15$ ns, $\tau_3 = 2.56$ ns

$[Ca^{2+}]$	α_1	α_2	α_3	f_1	f_2	f_3	$\cdot\ \bar{\tau}$ (ns)
0	0.837	0.163	—	0.496	0.504	—	1.40
	0.652	0.294	0.053	0.232	0.548	0.219	1.24
17 n*M*	0.808	0.192	—	0.447	0.553	—	1.49
	0.628	0.296	0.076	0.206	0.507	0.287	1.37
38 n*M*	0.778	0.222	—	0.402	0.598	—	1.58
	0.594	0.310	0.096	0.179	0.487	0.334	1.46
65 n*M*	0.755	0.244	—	0.371	0.628	—	1.64
	0.581	0.307	0.111	0.167	0.461	0.372	1.52
100 n*M*	0.745	0.255	—	0.359	0.641	—	1.66
	0.616	0.251	0.132	0.178	0.379	0.443	1.61
225 n*M*	0.651	0.349	—	0.263	0.737	—	1.84
	0.571	0.215	0.214	0.137	0.268	0.595	1.86
602 n*M*	0.499	0.501	—	0.160	0.840	—	2.04
	0.407	0.256	0.336	0.072	0.237	0.691	2.06
1.35 μ*M*	0.382	0.618	—	0.106	0.894	—	2.14
	0.364	0.181	0.455	0.055	0.143	0.801	2.23
40 μ*M*	0.305	0.695	—	0.078	0.922	—	2.19
	0.350	0.113	0.537	0.049	0.082	0.869	2.33

[a] See Table III footnotes for experimental details.

Table V. Multiexponential Analysis of the Intensity Decay of Calcium Crimson[a]

$[Ca^{2+}]$	$\bar{\tau}$ (ns)[b]	τ_i (ns)	α_i	f_i	χ_R^2	
0		0.83	0.462	0.195		
	2.51	2.92	0.538	0.805	2.5[c]	(127)[d]
		0.73	0.391	0.146		
		2.40	0.477	0.589		
	2.55	3.88	0.132	0.265	2.4	
100 n*M*		1.06	0.346	0.136		
	3.21	3.55	0.654	0.864	1.8	(67)
		0.97	0.302	0.109		
		2.04	0.373	0.409		
	3.23	3.99	0.324	0.482	1.9	
225 n*M*		0.93	0.280	0.087		
	3.54	3.79	0.720	0.913	1.6	(61)
		0.75	0.221	0.056		
		2.78	0.325	0.304		
	3.57	4.20	0.454	0.640	1.5	
602 n*M*		1.40	0.147	0.057		
	3.89	4.04	0.853	0.943	1.2	(10)
		1.02	0.085	0.024		
		3.09	0.316	0.268		
	3.91	4.32	0.598	0.708	1.2	
1.35 μ*M*		0.87	0.018	0.004		
	3.99	4.00	0.982	0.996	2.1	(2.1)
40 μ*M*		2.53	0.046	0.028		
	4.11	4.15	0.954	0.972	1.2	(1.3)

[a] Excitation, 590 nm, R6G dye laser; emission filter, Andover 610FG07 (transmits for > 610 nm); buffer, 100 m*M* KCl, 10 m*M* MOPS, 0–10 m*M* CaEGTA, pH 7.2, 20°C.

[b] $\bar{\tau} = \Sigma f_i \tau_i$.

[c] $\delta\phi = 0.3°$ and $\delta m = 0.005$.

[d] The values in parentheses are the χ_R^2 values from the single-decay time fits.

ters for the FLIM and FD measurements are listed in the figure legends and table footnotes.

Materials

Calcium Green (C-3010, Lot 22111, FW 1046), Calcium Orange (C-3013, Lot 22111, FW 1086), and Calcium Crimson (C-3016, Lot 22111, FW 1232) were obtained from Molecular Probes, Eugene, Oregon, and were used without further purification. Ca^{2+} concentrations were obtained using the Calibrated Calcium Buffer Kit II, also from Molecular Probes. All $[Ca^{2+}]$ refer to the concentration of free calcium. For FD measurements the temperature was 20°C. The FLIM measurements were done at room temperature, near 22°C.

RESULTS

Absorption and emission spectra of the three calcium probes are shown in Figs. 2–4. The shapes of the absorption and emission spectra are not changed in the presence of Ca^{2+}. Consequently, these probes cannot be used as ratiometric indicators. However, the fluorescence intensities increase in response to Ca^{2+} (Figs. 3 and 4). The intensity change is greatest for CaG (10.2-fold) and is smaller but still substantial for CaO (3.2-fold) and CaC (3.6-fold). We note that these enhancements are particularly suitable for FLIM measurements because the probes display detectable emission in the absence and presence of Ca^{2+}. If the probes were nonfluorescent in the absence of Ca^{2+}, then a lack of measurable intensity could be interpreted as being due to either no Ca^{2+} or no probe at a specific location. It is also important to recognize that the observation of a Ca^{2+}-dependent change in intensity does not necessarily imply that the lifetime will also be dependent on Ca^{2+}. For instance, if the intensity of the Ca^{2+}-free form of the dye is not significant, then the emission will be due to only the Ca^{2+}-bound form. Then, the lifetime will be that of the Ca^{2+}-bound form, independent of Ca^{2+} concentration. For this reason it is important to characterize the intensity decay of the probes, over a range of Ca^{2+} concentration.

Table VI. Global Multiexponential Analysis of the Intensity Decay of Calcium Crimson[a]

Double-exponential fit: χ_R^2 = 5.9 ns, τ_1 = 1.34 ns, τ_2 = 3.96 ns

Triple-exponential fit: χ_R^2 = 1.8, τ_1 = 0.79 ns, τ_2 = 2.55 ns, τ_3 = 4.14 ns

$[Ca^{2+}]$	α_1	α_2	α_3	f_1	f_2	f_3	$\bar{\tau}$ (ns)
0	0.732	0.268	—	0.479	0.521	—	2.70
	0.420	0.488	0.092	0.170	0.637	0.194	2.56
38 n*M*	0.608	0.392	—	0.343	0.657	—	3.06
	0.306	0.505	0.188	0.104	0.559	0.336	2.90
100 n*M*	0.473	0.527	—	0.232	0.768	—	3.35
	0.234	0.431	0.336	0.069	0.412	0.519	3.25
225 n*M*	0.344	0.656	—	0.150	0.850	—	3.57
	0.218	0.261	0.520	0.058	0.224	0.719	3.58
602 μ*M*	0.119	0.881	—	0.044	0.956	—	3.85
	0.071	0.165	0.764	0.015	0.116	0.868	3.86
1.35 μ*M*	0.005	0.995	—	0.002	0.998	—	3.96
	0.000	0.104	0.896	0.000	0.067	0.933	4.02
40 μ*M*	0.000	1.000	—	0.000	1.000	—	3.96
	0.002	0.025	0.973	0.000	0.016	0.984	4.10

[a] See Table V footnotes for experimental details.

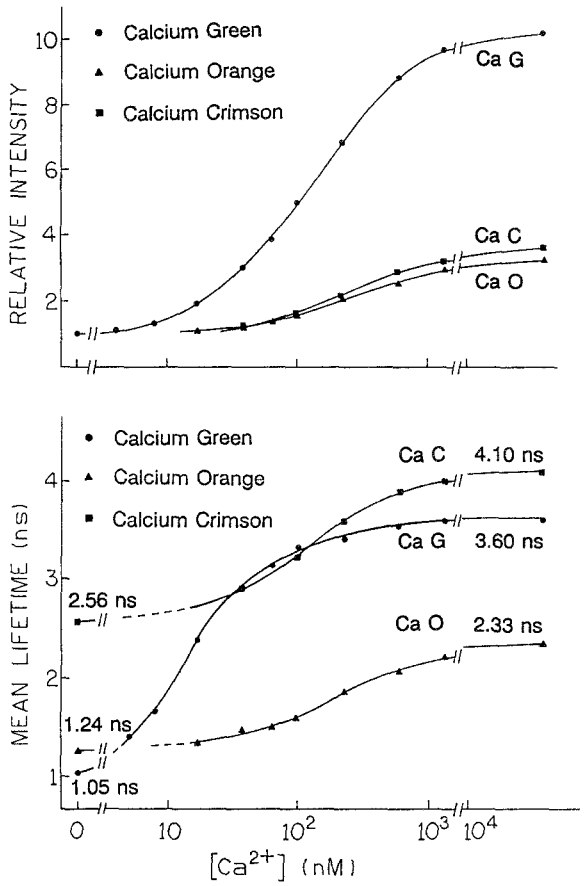

Fig. 7. Ca^{2+}-dependent fluorescence intensity (top) and mean lifetime (bottom) for Calcium Green, Orange, and Crimson.

We examined the intensity decay of the calcium probes using frequency-domain fluorometry. The Ca^{2+}-dependent frequency responses are shown in Figs. 5 and 6. In each case the frequency response shifts to lower frequency in the presence of calcium, with the largest shift being observed for CaG and less substantial shifts for CaO and CaC. The results demonstrate that the lifetimes of these probes are dependent on Ca^{2+} and that these probes are therefore suitable for FLIM.

The frequency-domain data were analyzed in terms of the multiexponential model. The intensity decays were all found to be complex, with the greatest degree of heterogeneity being observed for intermediate calcium concentrations or in the absence of calcium. This is illustrated for CaG in Table I. At calcium concentrations higher than 225 n*M* the decay is doubly exponential, with more than 95% of the intensity originating from the 3.7-ns component in the decay. At the intermediate calcium concentration of 38 n*M* the decay is strongly heterogeneous, as seen from the values of χ_R^2 from the single-decay time fits (Table I). Also, the data require three decay times for an adequate fit, with significant emission from the short (20- to 50-ps) and long (3.7-ns) components. Three decay times are also required to fit the CaG intensity decay in the absence of calcium (Table I). At present we are not certain whether the three decay times are intrinsic to the CaG probe. In the case of Quin-2 (21) we found that the intensity decay of a pure sample could be explained using just two decay times but that the presence of an impurity resulted in the appearance of a third decay time. A similar situation is possible for CaG. The third decay time could be the result of a fluorescent impurity, a species of CaG not responsive to calcium, or the presence of a trace amount of calcium in the presumed Ca^{2+}-free sample.

We reasoned that the same decay times should be present at all calcium concentrations but that the amplitudes (preexponential factor) should be Ca^{2+} dependent. This prediction is based on the probability that the emission rates are not altered by Ca^{2+}, in which case the α_i values represent the fraction of the fluorophore populations with the decay time τ_i. To test this prediction we performed a global analysis with global decay times but with α_i values which could be different for each $[Ca^{2+}]$. The triple-exponential global analysis results in a very reasonable value of χ_R^2 = 2.8 for CaG, whereas the global double-exponential fit results in an elevated value

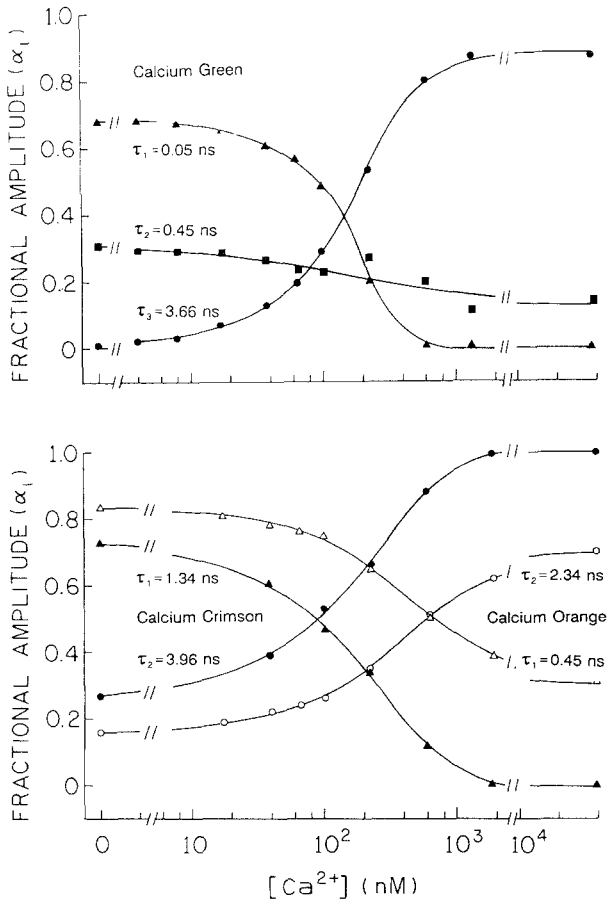

Fig. 8. Calcium-dependent preexponential factors for Calcium Green (top), Orange and Crimson (bottom).

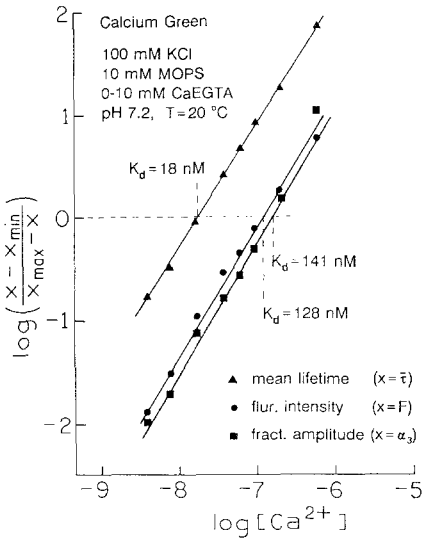

Fig. 9. Apparent dissociation constants of Calcium Green.

Table VII. Apparent Dissociation Constants of the Calcium Indicators[a]

Indicator	Apparent K_a (nM)[b]		
	Intensity	Amplitude	Mean lifetime
Calcium Green[c]	128 ± 1.5	141.0 ± 8.0	18.0 ± 0.5
Calcium Orange[d]	269 ± 2.0	389 ± 25	158 ± 2.0
Calcium Crimson[e]	283 ± 4.0	136 ± 1.0	117 ± 1.0

[a] Buffer 100 mM KCl, 10 mM MOPS, 0–10 mM CaEGTA, pH 7.2, 20°C.

[b] The dissociation constants were obtained from the intensity [Eq. (9)], the fractional amplitude in the multiexponential decay (Eq. (8)], or the mean lifetime (Eq. (10)].

[c] Fluorescence intensities were measured with excitation at 488 nm; amplitudes and mean lifetimes were measured with excitation at 514.5 nm. Emission was observed for ≥515 nm.

[d] Excitation, 565 nm; emission, ≥575 nm.

[e] Excitation, 590 nm; emission, ≥610 nm.

of χ^2_R = 86.2 (Table II). While the value of χ^2_R from the double-exponential analysis is poor, we chose to report the α_i and τ_i values from this fit because these are probably representative of what would be observed using a more highly purified sample of CaG and/or instrumentation with less resolution of complex decays. These result supports the use of the multiexponential model with calcium-dependent α_i values. However, we cannot exclude the possibility that the actual intensity decay is a distribution of lifetimes or of some other nonexponential form.

We also characterized the intensity decays of CaO and CaC. In both cases, the presence of Ca^{2+} resulted in an increase in the mean lifetime resulting from an increased amplitude of the longer lifetime component in the multiexponential decay (Tables III and V). Also, the Ca^{2+}-dependent decays of CaO (Table IV) and CaC (Table VI) were consistent with the global model in which the decay times are independent of calcium, but the amplitudes are Ca^{2+} dependent. Once again, the triple-exponential model was needed to account for the intensity decays of CaO, but the decay of CaO appeared to be less heterogeneous than that of CaG. Also, the decay of CaC was still less heterogeneous, and at high [Ca^{2+}] the double-exponential model accounted for the data.

The mean decay times from the multiexponential analyses are summarized in Fig. 7, which also shows the Ca^{2+}-dependent intensities of the three probes. One notices that the relative increase in intensity in response to Ca^{2+} is greater than the relative increase in lifetime.

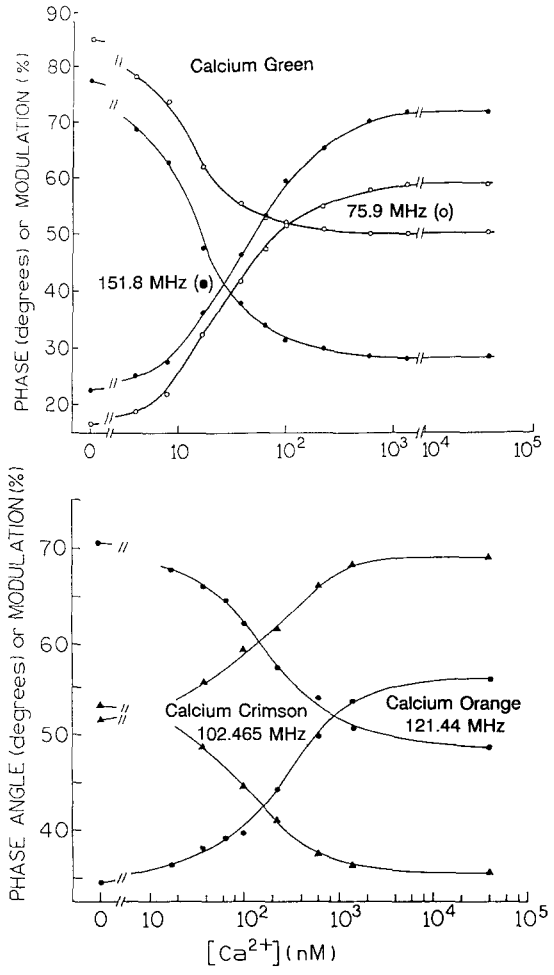

Fig. 10. Top: Ca^{2+}-dependent phase and modulation of Calcium Green at 75.9 and 151.8 MHz. Bottom: Ca^{2+}-dependent phase and modulation for Calcium Orange at 121.44 MHz and Calcium Crimson at 102.465 MHz.

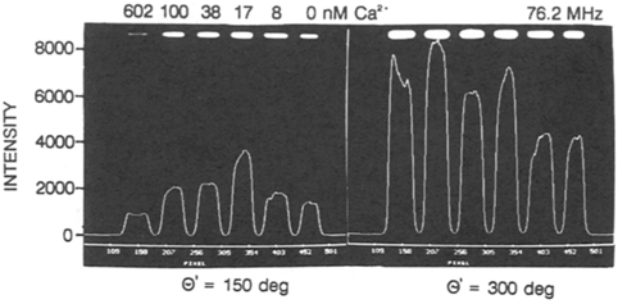

Fig. 11. Phase-sensitive intensities of Calcium Green collected with the FLIM apparatus. The data shown are for a single row of pixels in the center of the illuminated regions of the cuvettes.

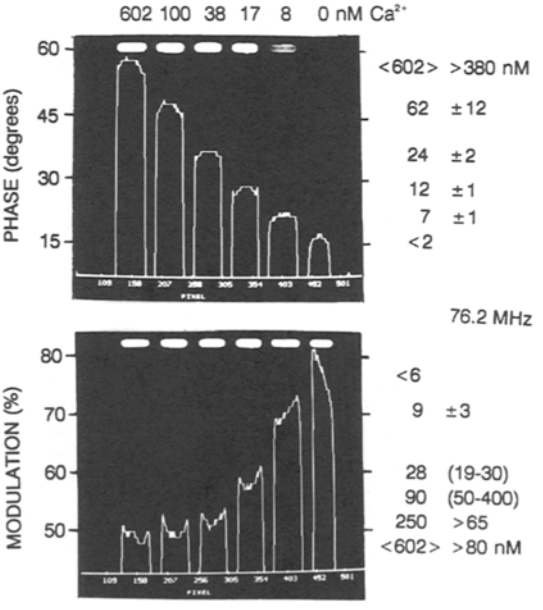

Fig. 12. Phase angle and modulation images of Calcium Green at 76.2 MHz.

This could be the result of the mean lifetime being weighted toward the longer-lived components in the decay, which are also more intense than the short-lived components.

The results from the multiexponential analysis can be used to calculate the Ca^{2+} dissociation constants for the Ca^{2+} probes. If one makes the reasonable assumption that binding of Ca^{2+} does not alter the emissive rate, then the preexponential factors represent the fractional population of each form of the probe. These values for the Ca^{2+}-dependent preexponential factors are shown in Fig. 8 for CaG (top) and CaO and CaC (bottom). In the case of CaG (Fig. 8, top), the value of α_3 increases and the values of α_1 and α_2 decrease with increasing amounts of Ca^{2+}. For the case of CaG, where the origin of the three decay times is uncertain, we assumed that $\alpha_1 + \alpha_2$ represents the fraction of the free probe, and the preexponential factor for the longest decay time (α_3) represents the fractional Ca^{2+} saturation of the indicator (Fig. 8). These Ca^{2+}-dependent amplitudes can be used to calculate the apparent dissociation constants (Fig. 9),

$$[Ca^{2+}] = K_D\left(\frac{F - F_{min}}{F_{max} - F}\right) \tag{9}$$

as can the mean lifetimes or intensities, using

$$[Ca^{2+}] = K_D\left(\frac{\alpha_3 - \alpha_{3min}}{\alpha_{3max} - \alpha_3}\right) \tag{10}$$

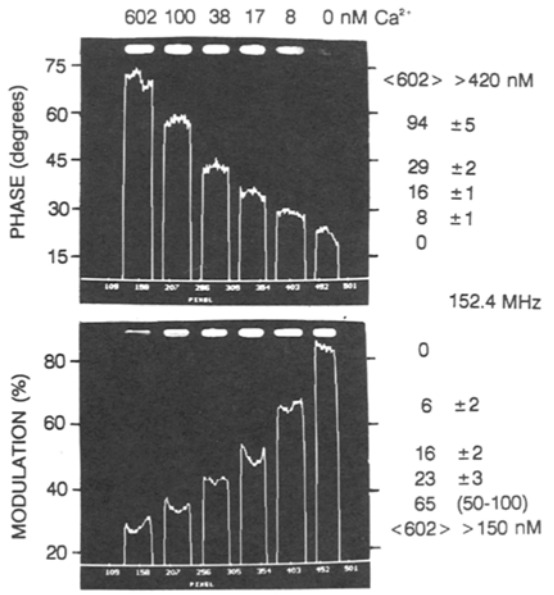

Fig. 13. Phase angle and modulation images of Calcium Green at 152.4 MHz.

or

$$[Ca^{2+}] = K_D\left(\frac{\bar{\tau} - \bar{\tau}_{min}}{\bar{\tau}_{max} - \bar{\tau}}\right) \quad (11)$$

In these expressions, the apparent values of K_D are not necessarily equal, F_i refers to the intensities (Fig. 7), and the τ_i refers to the mean lifetime (Fig. 7) obtained using

$$\bar{\tau} = \sum_i f_i\tau_i \quad (12)$$

In the case of CaO and CaC, the double-exponential model is nearly adequate to account for the intensity decays. Hence, we show (Fig. 8, bottom) the dependence of α_1 and α_2 on $[Ca^{2+}]$, where α_1 and α_2 are assumed to represent the fractional amounts of probe without and with bound Ca^{2+}, respectively.

The Ca^{2+} dissociation constants can be obtained from the intensities, amplitudes or mean lifetimes, as shown in Fig. 9 for CaG. The dissociation constant can be found from the *Y*-axis zero intercept. The Ca^{2+} dissociation constants are summarized in Table VII. The lower apparent value of K_D obtained from the mean lifetime is a result of the larger contribution of the higher-intensity Ca^{2+}–CaG complex to the mean lifetime. These dissociation constants are in reasonable but not precise agreement with those reported recently by Eberhard and Erne (22). The latter measurements were performed at different temperatures and over a range of pH values, and the author used only the intensity data. Hence, a detailed comparison of the K_D values is not warranted at this time.

Fluorescence Lifetime Imaging of Calcium Green

The FLIM measurements are presently performed using a single modulation frequency. Hence, it is of interest to examine the Ca^{2+}-dependent phase and modulation data at selected frequencies, in order to select an optimal frequency consistent with the lifetimes displayed by the samples and the useful frequency range of the FLIM instrumentation. Phase and modulation data for CaG, CaO, and CaC at selected frequencies are shown in Fig. 10. CaG displays the largest change in phase and modulation (Fig. 10), with very useful changes available from 70 to 500 MHz (Fig. 5). Somewhat smaller changes in phase and modulation are seen for CaO and CaC than for CaG, but these changes are more than adequate with the current precision of our FLIM instrumentation. Conveniently, all three calcium indicators show substantial shifts in phase and modulation at frequencies below 160 MHz, which is near the upper frequency limit of our FLIM apparatus. It is important to recognize that a calibration curve of phase or modulation versus Ca^{2+} concentration, such as those shown in Fig. 10, can be obtained irrespective of the multiexponential intensity decay. Also, resolution of the multiexponential decay parameters is not required for lifetime imaging or cell-by-cell Ca^{2+} measurements in flow cytometry.

It should be noted that the use of phase-modulation methods allows the apparent K_D values to be shifted by selection of the modulation frequency or type of measurement. For instance, the apparent K_D value from the phase data vary from 30 to 60 n*M* as the modulation frequency is increased from 75.9 to 303.6 MHz, and those from the modulation data change from 14 to 17 n*M* (not shown). Hence, a range of apparent K_D values can be obtained by modification of the experimental details.

We expect FLIM to be useful in fluorescence microscopy where it is not practical to perform single-wavelength intensity measurements. However, in the present study we imaged a row of six cuvettes, each with a different Ca^{2+} concentration. This allowed control measurements in which the same samples were measured with our standard frequency-domain instrumentation. Such control measurements are needed to verify the accuracy of the phase and modulation data obtained from the FLIM apparatus. The FLIM images are calculated

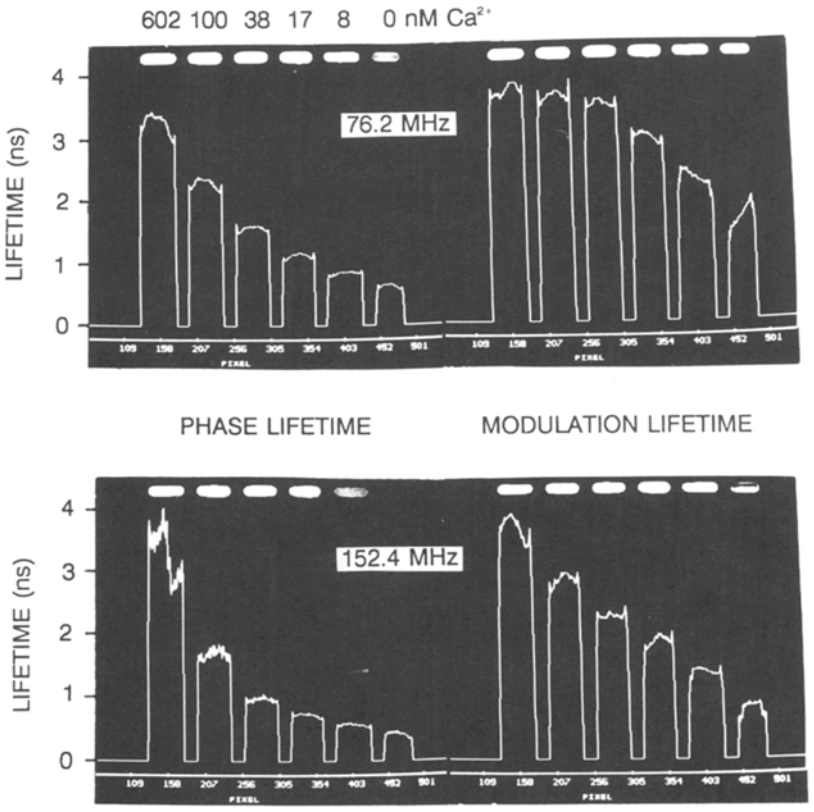

Fig. 14. Lifetime images of Calcium Green.

from a series of phase-sensitive images. Representative data are shown in Fig. 11, which shows the phase-sensitive intensities for a single row of pixels at the central part of the illuminated region of the cuvettes. One notices that the phase-sensitive images vary dramatically with the phase angle shift between the detector gain and the emission. For instance, the phase-sensitive intensities of the six samples vary in amplitude and relative to each other as the detector phase angle is changed from 150 to 300° (Fig. 11).

A series of phase sensitive images can be used to calculate a lifetime image. Images can be presented as a phase angle image or transformed into a phase lifetime image using Eq. (5). In Fig. 12, the heights of the lines are the phase angle (top) or modulation (bottom) of a line drawn through the central area of the illuminated region of the cuvettes. In calculating this values we performed calculations only for regions of the image where the steady-state intensity was 5% or greater of the peak intensity. As expected from Fig. 10, the phase angles increase and the modulation decreases with increasing concentrations of Ca^{2+}. Similar results were found at 152.4 MHz (Fig. 13), except that the phase and modulation changes were larger at this higher frequency. The phase and modulation images in Figs. 12 and 13 can be used to compute lifetime images (Fig. 14). These images show that the lifetimes increase in response to calcium. Perhaps more importantly, closer inspection of Fig. 14 shows that the apparent phase and modulation lifetimes are shorter at the higher frequency and that $\tau_p < \tau_m$. These are the classical results for a multiexponential decay, which indicates that in the future, it will be possible to use multifrequency FLIM to accomplish a multiexponential analysis on a pixel-by-pixel basis.

It is important to emphasize that obtaining the expected values for the phase and modulation of CaG requires correction for the position-dependent frequency response of the image intensifier. This position-dependent response was measured by placing a tube filled with dilute solution of R6G into the laser beam so that it occupied the same area as the cuvettes. The phase angle across the intensifier varied from the central to the outer circumference, as shown in Fig. 15. These intensifier-dependent phase shifts were used to correct the phase

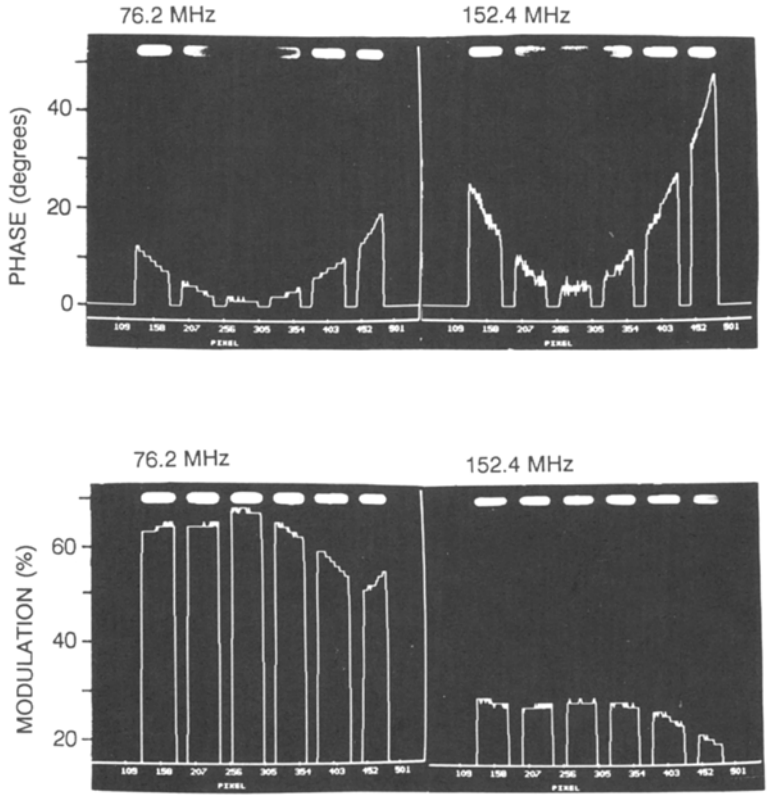

Fig. 15. Image intensifier correction curves. The sample was an axially illuminated tube of rhodamine 6G in water. Data are shown only where there was intensity from the six cuvettes.

Table VIII. Phase, Modulation, and Calcium Concentration from the FLIM and Frequency-Domain Measurements of CaG at 76.2 MHz

Sample, Ca^{2+} (n*M*)	Method	Phase (deg)	Modulation (%)	[Ca^{2+}] from FLIM (n*M*)	
				Phase	Modulation
0	FD	15.2	85.1	—	—
	CCDFT	16.1 ± 1.5	79.3 ± 4.3	<2	<6
8	FD	23.0	72.6	—	—
	CCDFT	21.3 ± 1.4	70.6 ± 3.3	7 ± 1	9 ± 3
17	FD	32.3	62.4	—	—
	CCDFT	27.7 ± 0.8	58.5 ± 1.9	12 ± 1	29 (19–30
38	FD	42.0	55.0	—	—
	CCDFT	36.3 ± 0.9	52.1 ± 2.1	24 ± 2	90 (50–400)
100	FD	51.5	51.8	—	—
	CCDFT	47.1 ± 1.8	50.4 ± 2.7	62 ± 12	250 (>65)
602	FD	57.7	50.2	—	—
	CCDFT	<58.0> ± 1.7	<49.6> ± 3.1	<602> (>380)	<602> (>80)

angles of CaG, resulting in the images shown in Figs. 12–14. The phase angles obtained following this correction are in good agreement with the values measured with our FD instrumentation (Tables VIII and IX).

Table IX. Phase, Modulation, and Calcium Concentration from the FLIM and Frequency-Domain Measurements of CaG at 152.4 MHz

Sample, Ca^{2+} (n*M*)	Method	Phase (deg)	Modulation (%)	[Ca^{2+}] from FLIM (n*M*)	
				Phase	Modulation
0	FD	22.5	77.3	—	—
	CCDFT	22.0 ± 0.6	86.3 ± 4.1	0	0
8	FD	28.2	62.5	—	—
	CCDFT	28.2 ± 0.8	66.4 ± 3.1	8 ± 1	6 ± 2
17	FD	36.2	48.5	—	—
	CCDFT	34.4 ± 1.2	50.2 ± 1.9	16 ± 1	16 ± 2
38	FD	46.5	37.5	—	—
	CCDFT	42.6 ± 0.6	43.1 ± 2.5	29 ± 2	23 ± 3
100	FD	58.9	31.8	—	—
	CCDFT	57.8 ± 0.8	33.7 ± 2.4	94 ± 5	65 (50–100)
602	FD	69.8	28.5	—	—
	CCDFT	<70.4> ± 2.1	<28.5> ± 2.4	<602> (>420)	<602> (>150)

One may question why a position-dependent correction was performed in these imaging studies but not in our previous measurements (16,21). In the previous studies, we used mostly lower modulation frequencies and a smaller number of samples imaged onto the central region of the intensifier. Consequently, the position-dependent phase and modulation were apparently more constant, and in fact, we did not notice the position dependence during some of the early experiments. We note that it should be easy and practical to correct for these effects during microscopy experiments. This can be accomplished by examination of homogeneous samples which display constant decay times.

It is difficult to present two-dimensional images using only a gray scale. Consequently, we developed a pseudocolor scale to image Ca^{2+}. These images are shown at 76.2 and 152.4 MHz in Figs. 16 and 17, respectively. In these images, it is easy to relate a given phase or modulation value to a particular [Ca^{2+}]. It is interesting to notice that the modulation lifetimes are generally longer than the phase lifetimes (bottom, Figs. 14 and 15), as is expected for a multiexponential decay (23,24). This suggests that it should be possible to use the decay heterogeneity in the lifetime images as part of the information content of FLIM. And finally, we note that the resolution of the FLIM images can be increased by use of a higher modulation frequency. The phase and modulation images at 152.4 MHz are shown in Fig. 17. The change in both phase (top) and modulation (bottom) in response to calcium is greater at this higher frequency. This results in higher resolution of the Ca^{2+} concentration, as can be seen from the more expanded Ca^{2+} scale on the right side of each figure.

DISCUSSION

Fluorescence lifetime imaging provides a new opportunity for chemical imaging of cells. At present, the selection of fluorophores for FLIM is not straightforward. For instance, the Ca^{2+} probes Fura-2 and Indo-1 (Lakowicz *et al.,* unpublished observation) showed only small changes in phase angles in response to Ca^{2+}. A previous report indicated that the lifetime of Fura-2 is not strongly dependent on Ca^{2+} (25) and the use of Fura-2 in cells is hindered by autofluorescence and other difficulties (26). The present report expands the usefulness of FLIM to include imaging of Ca^{2+} using visible excitation and emission wavelengths. Among these probes, Calcium Crimson can be used with excitation wavelengths of up to 630 nm, which will be advantageous, due to reduced autofluorescence and phototoxicity to the cells, and will also allow the use of less expensive light sources.

And finally, we note that it has recently become possible to measure fluorescence phase angles (phase lifetimes) of individual cells in a flow cytometer (27,28). The series of calcium probes characterized in the present report is ideal for such measurements because they can be excited with the argon ion lasers commonly used in flow cytometers, and the decay times are within the present resolution of phase-flow cytometers. Furthermore,

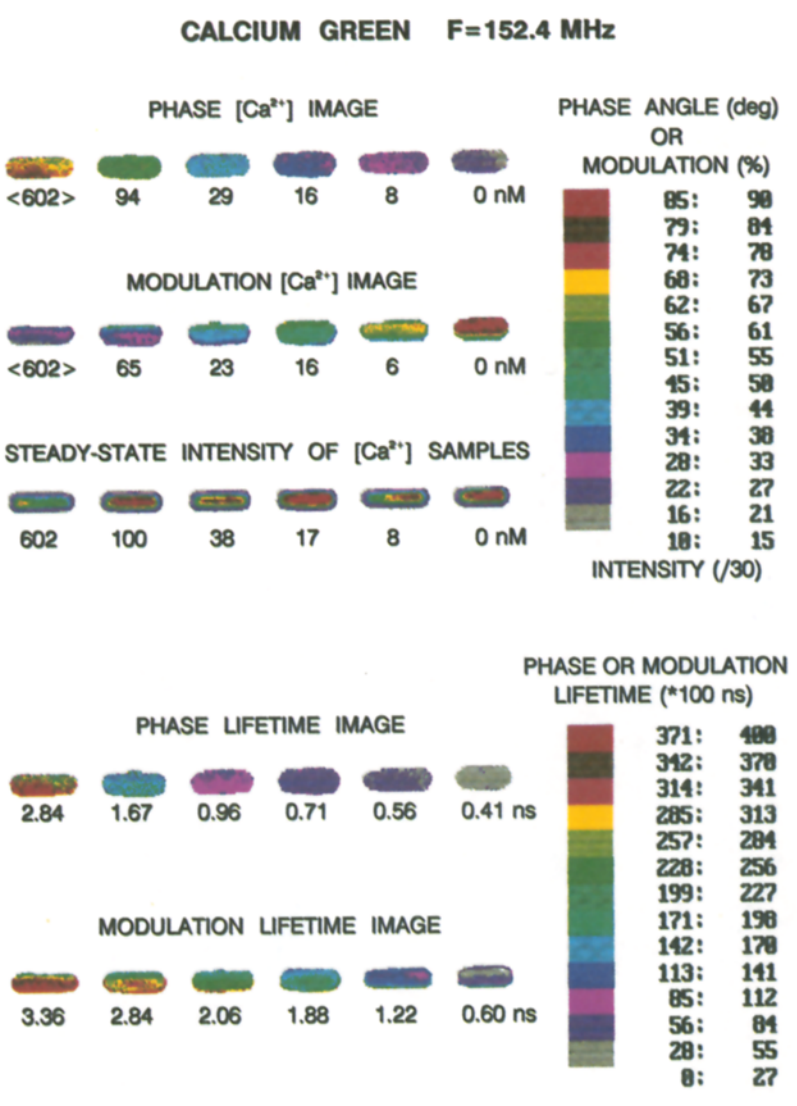

Fig. 16. Color imaging of Ca^{2+} at 76.2 MHz. The upper half shows the color-coded phase and modulation values. The Ca^{2+} concentrations obtained from the phase and modulation data are shown under each image. The $[Ca^{2+}]$ values under the steady-state intensity images are the known $[Ca^{2+}]$.

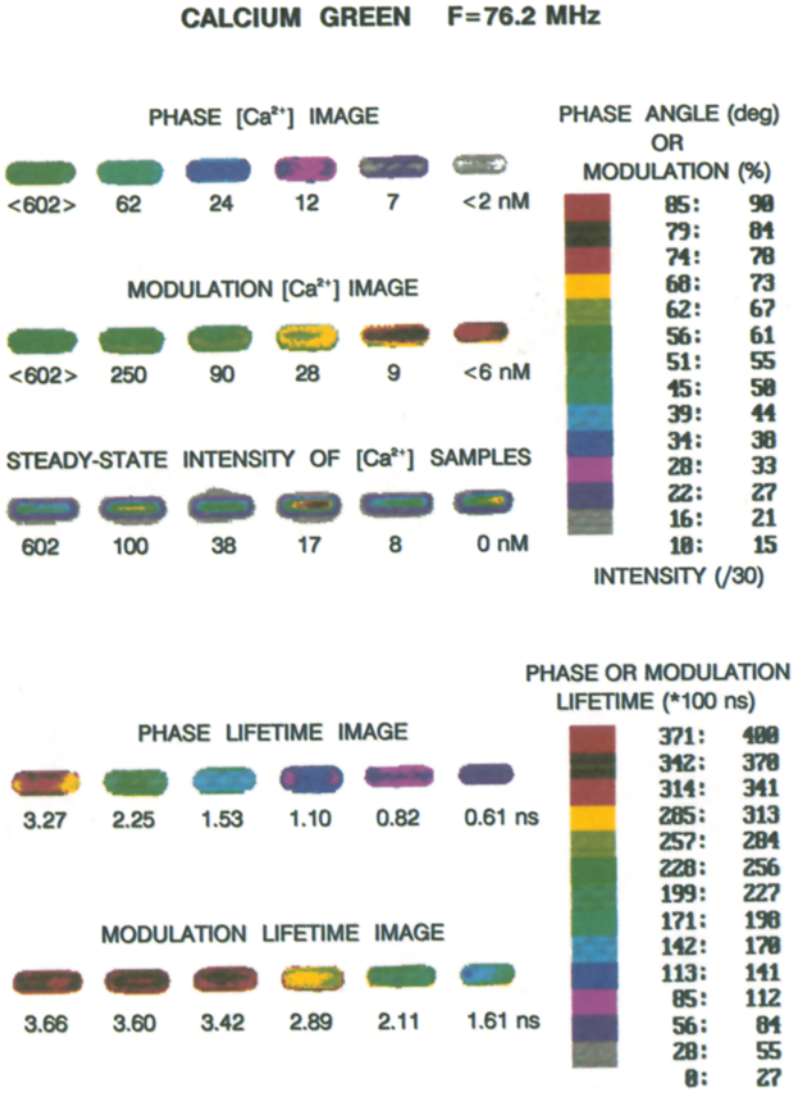

Fig. 17. Color images of Ca^{2+} at 152.4 MHz. See the legend to Fig. 16 for details. The phase and modulation values were corrected for position-dependent phase and modulation values (Fig. 15), as described for Figs. 12 and 13.

the three Ca^{2+} probes each display a different range of intensity and lifetime changes in response to Ca^{2+}, so that one of the probes can be selected as needed for the dynamic range of the phase flow cytometer and the desired range of Ca^{2+} concentrations. The capability to measure intracellular Ca^{2+} concentrations of individual cells rapidly will be a valuable research tool for cell physiology.

ACKNOWLEDGMENTS

The authors acknowledge support from National Science Foundation grants (DIR-8710401 and DMB-8804931), Center for Fluorescence Spectroscopy, the Medical Biotechnology Center and Graduate School of the University of Maryland, without whose support these experiments could not have been accomplished.

REFERENCES

1. R. Tsien (1980) *Biochemistry* **19,** 2396–2404.
2. R. Tsien and T. Pozzan (1989) *Methods Enzymol.* **172,** 230–262.
3. G. Grynkiewicz, M. Poenie, and R. Y. Tsien (1985) *J. Biol. Chem.* **260,** 3440–3450.
4. H. Komada, H. Nakabayashi, H. Nakano, M. Hara, T. Yoshida, H. Takanari, and K. Izutsu (1989) *Cell Struct. Funct.* **14,** 141–150.
5. E. D. Moore, P. L. Becker, K. E. Fogarty, D. A. Williams, and F. S. Fay (1990) *Cell Calcium* **11,** 157–179.
6. M. W. Roe, J. J. Lemasters, and B. Herman (1990) *Cell Calcium* **11,** 63–73.
7. W. F. Goldman, S. Bova, and M. P. Blaustein (1990) *Cell Calcium*.**11,** 221–231.
8. S. R. Adams, J. P. Y. Kao, G. Grynkiewicz, A. Minta, and R. Y. Tsien (1988) *J. Am. Chem. Soc.* **110,** 3211–3220.
9. J. H. Kaplan and G. C. R. Ellis-Davis (1988) *Proc. Natl Acad. Sci. USA* **85,** 6571–6575.
10. J. P. Y. Kao, A. T. Harootunian, and R. Y. Tsien (1989) *J. Biol. Chem.* **264,** 8179–8184.
11. Bioprobes (1991) No. 13, April, pp. 3–4.
12. Molecular Probes (1992) personal communication from Richard Haugland, April 6.
13. J. R. Lakowicz and B. P. Maliwal (1985) *Biophys. Chem.* **21,** 61–78.
14. E. Gratton and M. Limkeman (1983) *Biophys. J.* **44,** 315–324.
15. J. R. Lakowicz and K. W. Berndt (1991) *Rev. Sci. Instrum.* **62**(7), 1727–1734.
16. J. R. Lakowicz, H. Szmacinski, K. Nowaczyk, K. W. Berndt, and M. L. Johnson, (1992) *Anal. Biochem.* **202,** 316–330.
17. J. R. Lakowicz, H. Cherek, and A. Balter (1981) *J. Biol. Chem. Biophys. Methods* **5,** 131–146.
18. E. Gratton and M. Limkeman (1984) *Biophys. J.* **46,** 479–486.
19. J. R. Lakowicz, E. Gratton, G. Laczko, H. Cherek, and M. Limkeman (1984) *Biophys. J.* **46,** 463–477.
20. J. R. Lakowicz, G. Laczko, and I. Gryczynski (1986) *Rev. Sci. Instrum.* **57,** 2499–2506.
21. J. R. Lakowicz, H. Szmacinski, K. Nowaczyk, and M. L. Johnson (1992) *Cell Calcium* **13,** 131–147.
22. M. Eberhard and P. Erne (1991) *Biochem. Biophys. Res. Comm.* **180,** 209–215.
23. R. D. Spencer and G. Weber (1969) *Ann. N. Y. Acad. Sci.* **158,** 361–376.
24. J. R. Lakowicz and A. Balter (1982) *Biophys. Chem.* **16,** 99–115.
25. S. M. Keating and T. G. Wensel (1991) *Biophys. J.* **59,** 186–202.
26. E. D. W. Moore, P. L. Becker, K. E. Fogarty, D. A. Williams, and F. S. Fay (1990), *Cell Calcium* **11,** 157–179.
27. B. G. Pinsky and J. J. Ladasky (1992) *Proc. SPIE* **1640** (in press).
28. B. G. Pinsky, R. Hoffman, J. J. Ladasky, K. Berndt, and J. R. Lakowicz (1992) submitted for publication.